N94-22306

COMPARISON OF CLOUD MICROPHYSICAL PARAMETERS DERIVED FROM SURFACE AND SATELLITE MEASUREMENTS DURING FIRE PHASE II

David F. Young, Lockheed Engineering and Sciences Company, Hampton, VA 23666

Patrick Minnis, Atmospheric Sciences Division, NASA Langley Research Center, Hampton, VA 23681

Jack Snider and Taneil Uttal, NOAA Wave Propagation Laboratory, Boulder, CO 80302

Janet M. Intrieri and Sergey Matrosov, Cooperative Institute for Research in the Environmental Sciences, University of Colorado, Boulder, CO 80309

INTRODUCTION

Cloud microphysical properties are an important component in climate model parameterizations of water transport, cloud radiative exchange, and latent heat processes. Estimation of effective cloud particle size, liquid or ice water content, and optical depth from satellite-based instrumentation is needed to develop a climatology of cloud microphysical properties and to better understand and model cloud processes in atmospheric circulation. These parameters are estimated from two different surface datasets taken at Coffeyville, Kansas, during the First ISCCP Regional Experiment (FIRE) Phase-II Intensive Field Observation (IFO) period (November 13 - December 7, 1991). Satellite data can also provide information about optical depth and effective particle size. This paper explores the combination of the FIRE-II surface and satellite data to determine each of the cloud microphysical properties.

DATA AND ANALYSIS TECHNIQUES

The NOAA WPL 8.66-mm Doppler radar and an infrared radiometer were used to estimate ice water path (IWP) and mean ice particle diameter, D_e, over Coffeyville using the techniques of Matrosov et al. (1992). Optical depth was derived from the surface using the NOAA WPL 10.6-μm Doppler lidar whenever the cloud was thin enough to obtain a return signal from the stratospheric aerosol layer. Liquid water path was derived from data taken by an uplooking 2-channel microwave radiometer (Hogg et al., 1983). Visible (~0.65 μm, VIS), infrared (~11.0 μm, IR), and near-infrared (~3.8 μm, NIR) radiances from the NOAA Advanced Very High Resolution Radiometer (AVHRR) and the Geostationary Operational Environmental Satellite (GOES) were used to estimate effective ice crystal and water droplet sizes, and optical depth over the surface site and other locations. The AVHRR data were taken at 1-km resolution, while the GOES data resolutions varied from 4 to 16 km.

Bidirectional reflectance and effective emittances were computed for a variety of conditions using an adding-doubling radiative transfer model. Reflectances, $\rho_{vis}(\tau, r_e, \theta_o, \theta, \psi)$ and $\rho_{nir}(\tau, r_e, \theta_o, \theta, \psi)$, were computed for VIS optical depths, τ = 0.25, 0.5, 1, 2, 3, 4, 8, 16, 32, 64, 96, 128, for effective water droplet radii r_e = 2, 4, 6, 8, 12, 16, 32 μm, for randomly oriented hexagonal ice crystals in the cirrostratus (CS) and cirrus uncinus (CU) distributions (Takano and Liou, 1989) and for a full range of solar zenith θ_o, satellite zenith θ, and relative azimuth ψ angles. The NIR optical depths are $\tau_{nir} = \tau_{vis} Q_{nir}/Q_{vis}$, where Q is the extinction efficiency for a given wavelength and particle. The reflectances were compiled in lookup tables. The albedos for r_e = 6 and CS are shown in Fig. 1 for τ = 1 and 4. The CS albedo is much less than the water droplet model and is much less sensitive to changes in optical depth. Water droplet albedo decreases with increasing r_e. The same holds true for ice crystals. The CU model produces a smaller albedo than CS for the same optical depth. Optical depth is derived from a measured ρ_{vis} for a given model using the procedures of Minnis et al. (1993).

Effective emittance $\varepsilon(\tau, r_e, \theta, \Delta T)$ was computed for the same range of optical depths up to τ = 16, for the same particle size distributions, and satellite zenith angles as the reflectance calculations for the NIR and IR wavelengths. The emittances were computed for cloud temperatures T_c = 195, 220, 240, 255, 275, 285, 295K and for surface temperatures T_s = 260, 280, 300, 320K to yield a range in cloud-clear temperature differences ΔT = 5 to 125K for cirrus clouds and 5 to 80K for water clouds. The results were
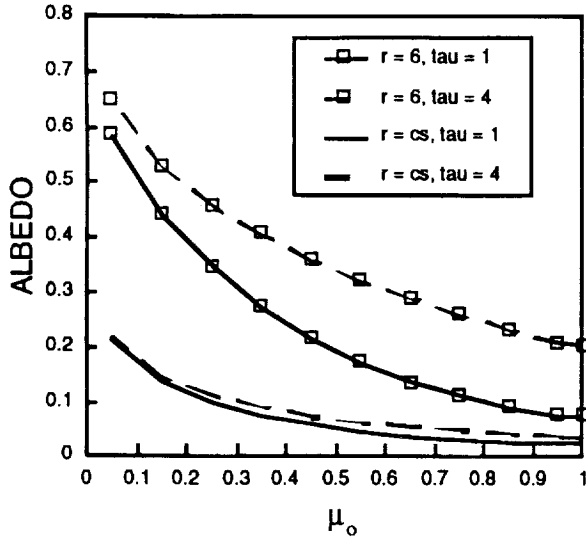
Fig. 1. Albedo for water droplet and cirrostratus ice crystal clouds at 3.73 μm from adding-doubling model computations.
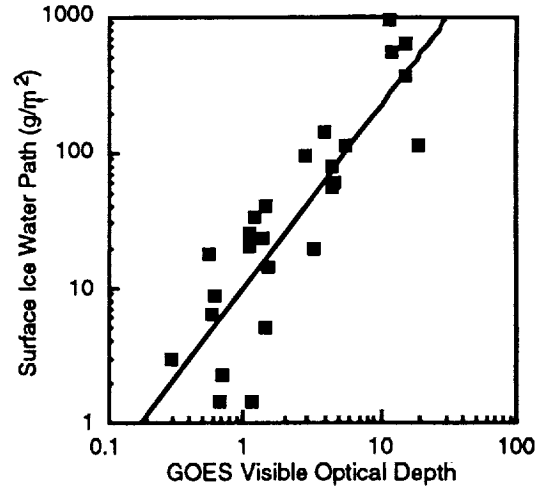
Fig. 2. Correlation of GOES-derived optical depth and surface-radar-derived ice water path for cirrus clouds over Coffeyville, Kansas during November 17 and 26, 1991.

parameterized as follows for a given wavelength λ.

$$\epsilon(r_e) = a_0 + a_1\{1/\ln(\Delta T)\} + a_2\{1/\ln(\Delta T)^2,$$

where $\mu = \cos\theta$, $a_i = S\ b_j\ \mu^j$, $j = 0, 4$ and $b_j = \Sigma\ c_k\ \mu^k$, $k = 0, 6$. The model standard error is $\pm 5\%$.

When only VIS and IR data are available, cirrus cloud optical depth and cloud-top temperature are derived as in Minnis et al. (1993) using the CS model. When all three channels are used, the particle size and optical depth are determined iteratively for each cloudy pixel similar to the method of Han (1991). The VIS-IR data are first used to determine the clear-sky temperature T_s. The models are used to compute sets of reflectance and emittance for each particle size and optical depth for the given pixel. The measured NIR and IR radiances are given in equivalent blackbody temperature $T\lambda$ where

$$B\lambda(T\lambda) = \epsilon\lambda\ B(T_c) + (1 - \epsilon\lambda)\ B(T_s) + \rho\lambda\ /\ \mu_o E\lambda, \qquad (1)$$

$\mu_o = \cos\theta_o$, and $E\lambda$ is the spectral solar constant which is zero for the IR channel. Effective radius, optical depth, and T_c are found simultaneously by solving (1) for the IR and NIR and matching τ to ρ_{vis} through the parameterization of Minnis et al. (1993). So far, the technique has only been used to determine r_e for water clouds and to simulate the radiances given T_c and either the CS or CU models.

RESULTS

GOES VIS and IR data were analyzed over Coffeyville to obtain the cirrus optical depth. In Fig. 2, the results for several days during November are plotted in a logarithmic scale with IWP derived from the radar data. This preliminary result shows that the two quantities are well correlated over the large range of IWP values. The linear logarithmic fit yields a much higher correlation than the simple linear fit. The scatter in this figure can arise from many sources including time and space mismatches between the surface and satellite, water cloud contributions to the optical depth, and variable particle sizes.

During December 5, the ER-2 flew missions over the Gulf of Mexico and over the hub. The ER-2 Gulf flight was coincident with the Landsat overpass at ~ 1030 LT. In the Gulf, scattered cirrus were observed over a layer of stratocumulus clouds. The NOAA-11 overpass occurred almost 4 hours later when cirrus cells could be seen over the stratocumulus clouds in the AVHRR imagery. A histogram of the effective radii derived using the AVHRR data over a portion of the stratocumulus field is shown in Fig. 3. The effective radii for cirrus-free scenes vary from 6 to 12 μm with an average of 10.2 μm. The mean radii ranged from 10 to 14 μm over the vicinity of the Landsat overpass. Figure 4 shows the 2-dimensional histogram of the channel 4 (10.8 μm) - channel 3 (3.7 μm) brightness temperature differences (BTD) plotted as functions of T_4. The VIS-IR analysis for this area showed that the lower and upper cloud layer had cloud-top temperatures of 275K and 247K, respectively. The curve corresponding to r_e = 12 μm plotted for the lower cloud shows that the data and the theoretical parameterizations are in
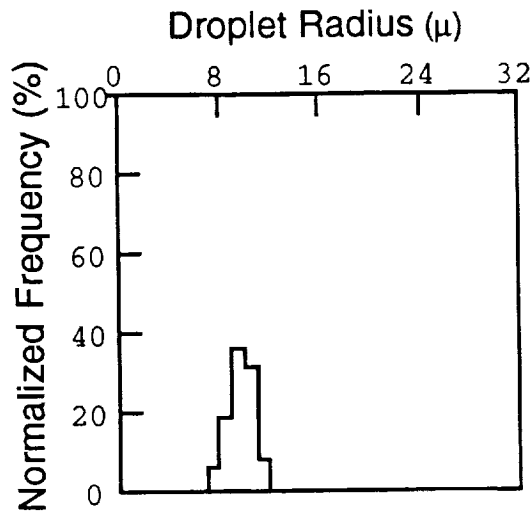
53

Droplet Radius (μ)

Fig. 3. Histogram of GOES-derived stratocumulus water droplet radius over the Gulf of Mexico from December 5, 1991.

Channel 4 T - Channel 3 T (K)

T4 Clear = 289.
T3 Clear = 288.
Tcloud = 275.
12 micron model

T4 Clear = 275.
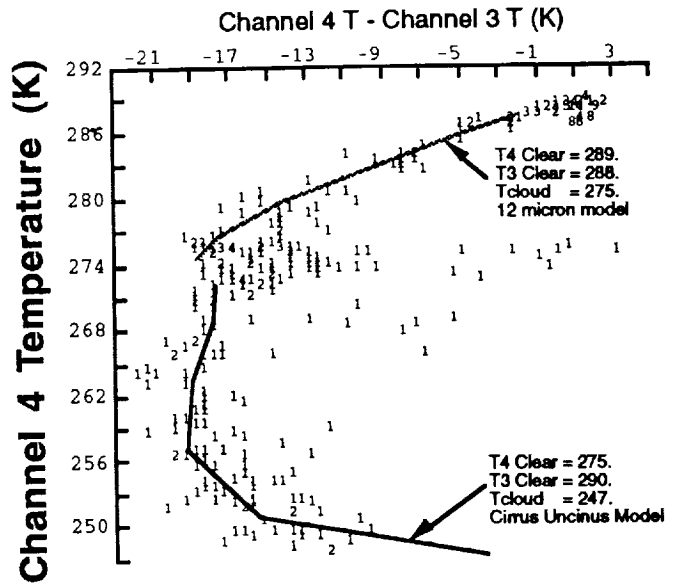T3 Clear = 290.
Tcloud = 247.
Cirrus Uncinus Model

Fig. 4. IR BTD histogram of cirrus uncinus over a stratocumulus layer.

excellent agreement. Since the high cloud is over the lower cloud and not over clear ocean, $T_S = 275K$ in (1) for the high cloud. The cirrus uncinus model produces an excellent fit to the data for the colder cloud. In the imagery, the high cloud shows the gross characteristics of cirrus uncinus, a dense head with streamers from the bottom. The pixels with $T_4 = 275K$ and BTD > -5K are apparently low clouds shadowed by the higher clouds. Low clouds without solar illumination typically have BTD $\geq$ 0. Fitting a single model to the cirrus clouds over Coffeyville met with less success as shown in Fig. 5. Surface lidar data indicate that the tops of the clouds at 2130 UTC varied from 11.3 to 12.1 km or 218 to 211K, while the bottom of the clouds ranged from 9.5 to 9.7 km or 231 to 230K. Using a single value of $T_c = 224K$ yields the curves shown in Fig. 5. The CS model appears to fit the thinner clouds quite well compared to the CU model. Thicker or higher clouds corresponding to the colder temperatures do not follow the CS model indicating that the cloud temperature was too warm or the effective crystal diameter was too large for the colder or thicker clouds. An iterative approach having a full spectrum of crystal sizes like the water droplet method is needed to fit these data.
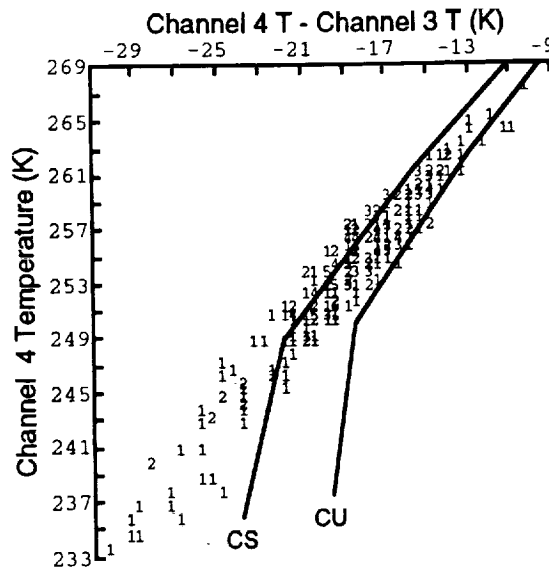
Channel 4 T - Channel 3 T (K)

Fig. 5. IR BTD histogram over Coffeyville, December 5, 1991.

DISCUSSION

Optical depth is related to the effective particle cross-sectional area and thickness of the cloud. Ice or liquid water path is related to the mean volume of the cloud particle distribution and the cloud thickness. Since the cross-sectional area is related to volume by the geometry of the particle, IWP or LWP is related to τ via the size and shape of the particle. Given the gamma size distribution for spheres, LWP can be approximated as $2\tau r_e/3$. This formulation is the basis for deriving r_e using the surface microwave LWP and the VIS optical depth. The relationship is not likely to be as simple for ice crystals because of the wide variety of shapes and sizes of particles within cirrus clouds. The results in Fig. 2 are encouraging, especially if it is possible to include the effective ice crystal size in the formulation.

The initial retrievals of r_e using the multispectral data are also encouraging but they highlight some of the difficulties that will be encountered in any application of the methodology. Selection of ice or water droplet models is straightforward if the cloud-top temperature is warmer than 273K or colder than 233K. For the many clouds having temperatures between 233 and 273K selecting the correct set of models is more complicated. While there may be some overlap in albedos for very small ice crystals and large water droplets, it may be possible to use the marked differences between the water droplet and ice 3.7-μm albedos (e.g., Fig. 1) to select the proper model set. A greater problem for applying the multispectral technique is the selection of the background radiating temperature. If only one layer is present in the scene, the use of the clear-sky temperature is warranted for all pixels. For the frequent occurrences of multilevel and convective clouds, it is necessary to know the characteristics of the background clouds. The large range in BTD for the pixels near T = 275K indicates that background clouds, even for a single contiguous stratus, can have variable optical properties. Deciding whether a pixel contains a thin cloud over a lower layer or a thick cloud at higher layer may also produce some ambiguities. The cloud shadowing seen in Fig. 3 also presents some logic challenges for automating the analysis procedures.

CONCLUDING REMARKS

Only a small portion of the FIRE-II lidar and radar IWP datasets has been used here. Combination of the remainder with the satellite products should provide a dataset large enough for an initial parameterization of IWP in terms of τ. Effective cirrus ice-crystal sizes may also be derivable using the multispectral data. The parameterization of IWP would probably be more reliable if the ice crystal size were included in the formulation. The surface-based LWP measurements (not shown here) will be used to estimate a value of r_e that may be a better representation of the entire cloud than the multispectral value. The latter may be highly dependent on the microphysics at the top of the cloud. The surface-based LWP data will also aid in determining the contributions of the water clouds to the satellite-observed radiances in the mixed phase and multilevel cloud systems observed during the IFO. In the future, these results will be compared to the FIRE-II in situ measurements to ensure the validity of the satellite and surface-derived quantities.

REFERENCES

Han, Q., 1992: Global survey of effective particle size in liquid water clouds. Ph.D. Dissertation, Columbia University, New York, NY, 199 pp.

Hogg, D. C., F. O. Guiraud, J. B. Snider, M. T. Decker, and E. R. Westwater, 1983: A steerable dual-channel microwave radiometer for measurement of water vapor and liquid in the atmosphere. *J. Appl. Meteorol.*, **22**, 789-806.

Matrosov, S. Y., T. Uttal, J. B. Snider, and R. A. Kropfli, 1992: Estimation of ice cloud parameters from ground-based infrared radiometer and radar measurements. *J. Geophys. Res.*, **97**, 11,567-11,574.

Minnis, P., P. W. Heck, and D. F. Young, 1993: Inference of cirrus cloud properties from satellite-observed visible and infrared radiances. Part II: Verification of theoretical radiative properties. *J. Atmos. Sci.*, **50**, 1305-1322.

Takano, Y. and K. N. Liou, 1989: Radiative transfer in cirrus clouds: I. Single scattering and optical properties of oriented hexagonal ice crystals. *J. Atmos. Sci.*, **46**, 3-20.